AIAA JOURNAL
Vol. 38, No. 1, January 2000

Measurement of Transient Temperature Field Within a Falling Droplet

QingZheng Lu* and Lynn A. Melton†
University of Texas at Dallas, Richardson, Texas 75083-0688

Fluorescence shift thermometry has been combined with droplet slicing imaging to capture images of the transient temperature field within a 500-μm-diam decane droplet falling into 370–420°C nitrogen. The temperature field becomes almost homogeneous within 5–10 ms of entry into the hot ambient gas and rises toward the boiling point of the liquid over 50–100 ms. The constraints faced in the design of such an experiment and the protocols required for successful measurement of such temperature images are addressed.

I. Introduction

DETAILED understanding of the processes that govern the heating and evaporation of individual droplets is important to understand the heating and evaporation of fuel sprays, which are composed of millions of droplets of varying sizes and velocities. Indeed, calculations of the suitability of various spray nozzles and patterns for use in combustors are often based on averages of the results for individual droplet trajectories. The processes assumed to control the behavior of individual droplets find their way, through these averages, into predictions for industrially important combustion processes.

Droplet heating, evaporation, and combustion have been the subject of a variety of theoretical[1–5] and experimental studies.[6–9] Theoretical studies often neglect the internal heat and mass transport within the droplet, and, so far as is known to the authors,[10] although methods for measurement of the temperature of droplets have been described,[11,12] there have been no other measurements of the transient temperature field within a droplet.

This paper describes fluorescence-based experimental methods that can be used to measure nonintrusively the transient temperature field within heating and/or evaporating hydrocarbon droplets. The temperature field is likely to be the key element in understanding the droplet heating and/or evaporation processes: It incorporates the internal transport processes that affect the surface temperature, a major parameter in determining the droplet vapor pressure and evaporation rate.

The combination of droplet slicing imaging (DSI), fluorescence shift thermometry (FST), and restoration of DSI images, which has been used in the present work, has been developed over a decade. In this paper, the three techniques are used together to capture temperature images within a falling hydrocarbon droplet that is undergoing heating.

Prior experimental and theoretical work indicates that imaging of the temperature field within the droplet is likely to give the most reliable and interpretable results. Wells and Melton argued that they measured the temperature of the outer portion of a falling droplet, the skin temperature, by using a solution with very high optical density, that is, the illuminating laser light was limited in its penetration of the droplet to the outer quarter of the radius of a 220-μm-diam droplet.[13] Hanlon and Melton used a much lower optical density and argued that their results yielded approximately a volume averaged temperature.[14] Zhang and Melton reanalyzed the Hanlon and Melton experiment and found that the imaging properties of the droplet resulted in an optical weighting of the fluorescence and consequent systematic errors in the inferred temperatures.[15] They concluded that estimation of a volume averaged temperature was likely to give significant systematic errors under transient conditions, and thus they recommended that imaging of the droplet temperature field was the method most likely to give reliable, interpretable results that would lead to better understanding of droplet heating. In a second paper, Zhang and Melton provided algorithms and programs to correct the DSI images for the optical distortion caused by the front-half of the droplet, which acts as a bad lens.[16]

Winter reported preliminary measurements of the temperature field in a falling droplet.[17] However, in that work, the droplet had fallen sufficiently far in the heated gas that the internal temperature field appeared to be homogeneous, and no information was obtained about the time-scale for establishment of the homogeneous temperature field.

This work is believed to be the first in which the transient, inhomogeneous temperature field in a falling droplet has been followed as a function of fall distance in the heated ambient gas. The droplet-to-droplet reproducibility of the system allows the images obtained on separate droplets at increasing fall distances (fall times) to be interpreted as if they were a time sequence obtained for a single heating droplet. It is hoped that the experimental methods developed will prove useful to others interested in the heating and evaporation behavior of droplets and that, through extensions of this work, a clearer understanding of the processes that govern droplet and spray heating and evaporation can be obtained.

II. Experimental

A. Design Constraints

The experiment as carried out had to meet severe design constraints. These are discussed here to provide an overview of the experiment.

For droplet temperature imaging, the fall tube and heater must 1) provide an almost instantaneous transition from room temperature to an (ideally uniform) hot zone, where the droplet is heated while it falls, 2) provide optical access to the falling droplet throughout its trajectory, 3) minimize the accumulation of hydrocarbon vapor, 4) minimize turbulence, and 5) for oxygen-sensitive fluorescence thermometers, provide an oxygen-free environment. Four of the five conditions just listed for the fall tube and heater system are related to the nitrogen flow rate. A higher flow rate provides a hotter and more nearly air- and hydrocarbon vapor-free environment, but it also leads to greater turbulence. Hence, the fall tube must be carefully designed, and the nitrogen flow rate must be carefully controlled to meet these constraints.

The calculation of the temperature field within the droplet requires that two pairs of images be ratioed pixel-by-pixel. Accurate determination of these ratios requires that 1) droplet trajectories be extremely reproducible, that is, negligible turbulence, and 2) the dual imaging optics be carefully aligned and insensitive to perturbations.

The choice of fluorescent thermometry molecule is also constrained. It must 1) be soluble in hydrocarbons, 2) have a spectrum

Received 6 July 1998; revision received 28 April 1999; accepted for publication 3 May 1999. Copyright © 1999 by the American Institute of Aeronautics and Astronautics, Inc. All rights reserved.

*Research Associate, Department of Chemistry; also Associate Professor, Department of Modern Chemistry, University of Science and Technology of China, Hefei, 230026 Anhui, People's Republic of China. Deceased.

†Professor, P.O. Box 830688, Department of Chemistry.

that changes significantly with temperature, 3) be strongly absorbing and fluorescing, and 4) absorb and emit in spectral regions that are appropriate for laser excitation and charge-coupled device (CCD) detection, respectively. Ideally, its fluorescence intensity should also be insensitive to oxygen. As a further molecular constraint, Winter and Melton[18] found that the best reasonably uniform illumination of a droplet (and thus, accurate determination of the temperature field) is achieved when the droplet optical density [(DOD) equal to absorbance across the diameter of the droplet] is approximately 1.

B. Chemicals

The 1,3-bis [1′-pyrenyl] propane (PYPYP) was obtained from Molecular Probes, Inc., and was used as received. Decane (99+%) was purchased from Aldrich and was used as received. Nitrogen gas (99.99%) was purchased from Air Liquide. Cobalt(II) sulfate was purchased from Alfa Products.

C. Experimental Apparatus

In this work, two experimental techniques have been combined to obtain the temperature field within a droplet: DSI[18,19] and FST.[20] For DSI, a thin laser sheet is used to illuminate the central plane of a droplet, and the droplet images are recorded by a CCD camera, commonly at a right angle to the incident laser beam. Hence, the firing of the laser, the droplet fall time, and the CCD exposure gate must be synchronized. For FST, the fluorescence of the dopant in alkane shifts to higher energy as the temperature increases, and the ratio of the intensity in a band at the blue edge of the fluorescence band to that in a band farther to the red can be calibrated as a function of temperature and can be used as a noncontact thermometer. To use this technique with falling droplets, the DSI fluorescence image of the droplet is split into two images by a roof prism so that two images are captured on the CCD. The light for one image passes through a blue filter, and the light for the other passes through an orange filter. A pixel-by-pixel ratio of the intensities in these two images, in conjunction with the temperature calibration curve, yields the spatially resolved temperature distribution within the droplet.

A block diagram of the experimental apparatus is shown in Fig. 1 with the fall tube shown from the top. A side view of the fall tube is shown in Fig. 2. In the discussion that follows, the x axis is horizontal and parallel to the laser beam ($+x$ is away from the laser), the y axis is horizontal and perpendicular to laser beam ($+y$ is toward the CCD camera), and the z axis is vertical ($+z$ is down, the droplet fall direction).

1. *Timing*

The timing of the devices is conceptually simple: A pulse forces a droplet out of the droplet generator and, after a variable delay time, the CCD camera exposure is gated on, and the YAG laser fires. The

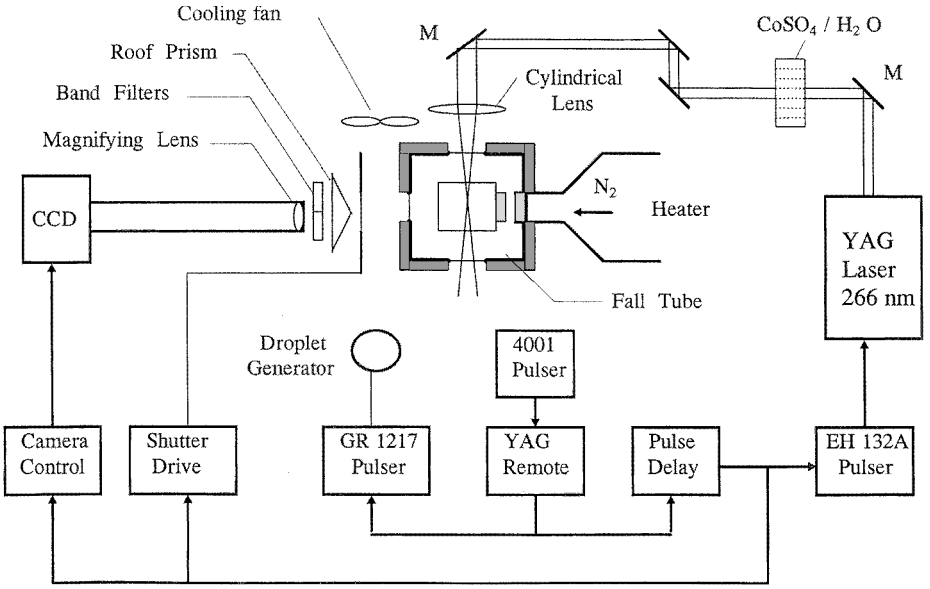

Fig. 1 Block diagram of apparatus; top view of fall tube.

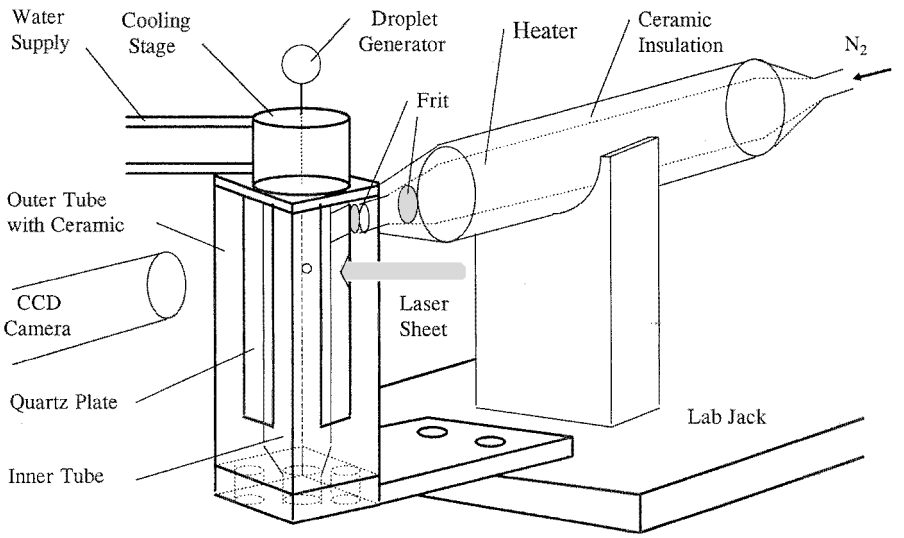

Fig. 2 Fall tube apparatus, side view.

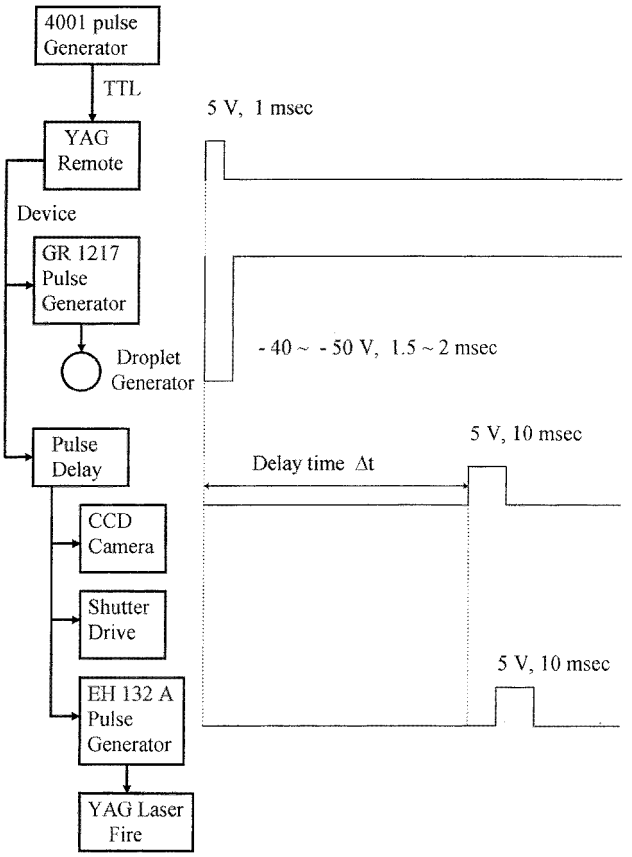

Fig. 3 Timing of pulses.

virtually instantaneous fluorescence is captured, the CCD exposure is gated off, the data are transferred to the controller computer, and the experiment is repeated as required. However, the YAG laser had a fixed 1-Hz cycle for firing its flashlamps, and thus the implementation of the timing sequence required that the other parts of the apparatus be synchronized to the YAG laser. The droplet generator was driven by a 40–50 V pulse, 1–2 ms in duration. The minimum exposure time for the CCD was 100 ms. To minimize background from the heater incandescence, a shutter that was open for 10 ms (triggered by a 5-V, 10-ms pulse) was placed in front of the CCD system; the laser fired 2–3 ms after the triggering of the shutter. The experiment was repeated after a delay of 9 s. Figure 3 shows the timing sequence.

2. Light Source and Excitation Optics

The output from the fourth harmonic (266 nm) of a Q-switched Nd:YAG laser [full width at half maximum (FWHM) 10 ns, about 2 mJ/pulse] was reflected by dielectric mirrors (266 nm 45 deg, CVI Laser) and then focused by a quartz cylindrical lens ($f = 8$ cm) into a thin sheet. The cylindrical lens was mounted on a dual-axis (x and y) translation stage (Lansing) that could be adjusted with micrometers to align the laser sheet to the droplet. The FWHM of the YAG 266-nm laser sheet in the y direction was 50–60 μm [measured by scanning the laser beam across a thin metal slit positioned in front of a laser power detector (ScienTech; MA10)].

Some of the green 532-nm light remained in the 266-nm beam, even after the laser beam had passed through the wavelength separation prism. Although the intensity at 532 nm was much less than that at 266 nm, the scattered 532-nm light interfered with the detection of the PYPYP fluorescence, which peaked at 498 nm. A 1-cm quartz cell filled with $CoSO_4/H_2O$ solution (240 g/l, bandpass 230–400 nm) was placed in the laser pathway as a filter, and the interference from the 532-nm light was eliminated.

3. Fall Tube and Heater

The fall tube used was similar to that used by Hanlon and Melton,[14] but it was redesigned and rebuilt to allow for cleaning of the optical components and replacement of the frits. The fall tube apparatus consisted of two square channels (see Figs. 1 and 2), the outer tube was aluminum (outer dimensions 3.8 × 3.8 × 15 cm, 3 mm thick), and the inner one was quartz (1.2 × 1.2 × 17 cm, 1 mm thick). Each of three sides of the outer tube had a narrow slot (1 × 10 cm) covered by a quartz plate (1.8 × 10.6 cm, 2 mm thick) that was clipped to the aluminum wall and that provided optical access, whereas near the top of the fourth side, there was a hole (1.2 cm diameter) where the heater outlet was inserted. The aluminum outer tube had insulation (outer dimensions 5 × 5 × 15 cm) made of machinable ceramic plates (McMaster–Carr Company). The top of the fall tube had a square ceramic cover (4 mm thick) with a hole (3 mm diameter) at the center for droplet entry. The bottom of the fall tube had a square ceramic plug (20 mm thick). The top end of the inner tube fitted into a 2-mm-deep groove in the top cover, and the conical bottom end of the inner tube fitted into the central hole of the bottom ceramic plug. A water-cooled cylindrical brass stage (50 mm diameter 45 mm height) sat on the cover of the fall tube; it had a hole (3 mm diameter) along its axis. The cooling stage and fall tube were clamped together so that they could be aligned and subsequently moved as a unit.

The heater was a quartz tube (2.4 cm o.d., 15 cm long), filled with fire brick fragments and heated externally by a cylindrical ceramic fiber heater (Watlow; 12 cm long, 550 W at 120 V; Model VC401E120A). The heater was covered by a layer of ceramic fiber insulation (Kaowool, 10 cm thick), and the heater and insulation were encased in a metal sheet. A 220-V variable transformer was used to supply electric power to the heater; under typical operating conditions, 110–130 V was supplied to the heater. Two quartz frits, one on the heater outlet and the other on the side of the inner tube that faces the heater, diffused the nitrogen flow. In this manner the major portion of the heated nitrogen heated the chamber between the inner and outer tubes, and the minor portion flowed downward through the inner tube to purge hydrocarbon vapor and ambient air from the inner tube. The ambient temperature inside the fall tube was measured with a digital thermometer (OMEGA; HH82) with J-type iron-constantan thermocouple that could be inserted into the fall tube from the bottom.

The assembled fall tube and heater, the droplet generator, and the solution reservoir were mounted on a high-quality laboratory jack (three orthogonal hinges, 400-lb capacity Newport; M280), so that they could be moved vertically (z direction) and smoothly as a single unit. All optical devices are kept on a fixed table. The droplet imaging at different fall distances was accomplished by adjusting the jack up or down and by changing the delay time.

The total nitrogen flow was measured and controlled with a rotameter (Matheson, tube 605). The ceramic plug at the bottom of the fall tube had five holes for nitrogen flow; the central one was for the inner tube, and the four others were for the outer tube. One or more of the four outer holes could be blocked to manipulate the ratio of nitrogen flow in the outer tube to that in the inner tube. At a total flow rate at 15 ml/s, with three outer holes blocked, the flow rate through the inner tube was 6.2–6.6 ml/s, as measured with a soap film flowmeter (AllTech; 25 cm^3) and a stopwatch. The full length of the inner tube was 17 cm, and thus at this flow rate, the inner tube was purged in approximately 3 s, one-third of the 9-s interval between droplets. An ambient atmosphere free of hydrocarbon vapor was provided for each droplet. This flow rate had little effect on the stability of the droplet position for fall distances up to 20 mm, but it caused variability in the droplet trajectory for greater distances.

In this apparatus, the maximum ambient temperature in the inner tube was 420°C; under those conditions the temperature in the outer tube was 570°C, which approached the melting temperature of aluminum (650°C). A subsequent apparatus was constructed of stainless steel.

4. Droplet Generator

The simple and reliable droplet generator used is shown in Fig. 4. The generator body was made of a copper ring (2.5 cm o.d., 1.8 cm i.d., and 0.8 cm long). A glass window was epoxied to one side of the copper ring, and a miniature piezoelectric buzzer element (Radio Shack; catalog number 273-064) was epoxied to the other side. At

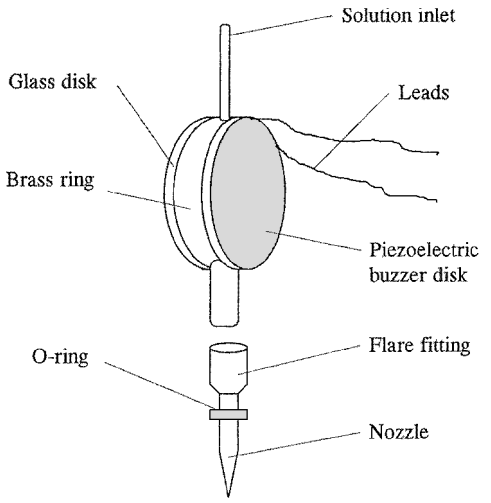

Fig. 4 Piezoelectric disk droplet generator.

the top of the ring, a piece of copper tubing (3-mm o.d., 1.5 cm long) is soldered to the ring as the solution inlet. It was connected with metal tubing (plastic tubing is porous to oxygen) to the glass solution reservoir. The droplet nozzle was a straightened MicroTorch welding tip with a laser-drilled ruby orifice (Smith Corporation; part number 129-124-03, orifice 279 μm). It was attached by means of a flare fitting soldered to the bottom of the ring. The tip of the droplet generator was inserted into the central hole of the cold stage, and an O-ring was used to make a seal that is sufficient to prevent hot nitrogen in the fall tube from traveling upward. (Such an upward flow of hot nitrogen would heat the droplet generator and cause additional turbulence in the fall tube.) The droplet generator was clamped to a two-axis (x and z) Newport M423 translation stage.

The height of the solution level in the reservoir relative to the droplet generator nozzle was critical for proper droplet production: The former had to be 2–3 mm higher than the latter. The reservoir was placed on a small jack, and its height could be adjusted. The PYPYP/decane solution in the reservoir was purged with nitrogen to remove dissolved oxygen.

A voltage pulse of approximately 45 V was sufficient to produce droplets. Slightly higher voltages yielded satellite droplets. With a nozzle orifice of 279 μm, decane droplets of approximately 500 μm diameter were generated.

5. CCD Camera and Imaging Optics

Droplet images were taken with a two-dimensional CCD camera (Photometrics; STAR I). It was mounted on a combined translation stage that included a dual-axis stage (Newport, M400) for horizontal motion (x–y direction) and a single-axis stage (Newport, M423) for vertical motion (z direction). To magnify the droplet images, an aluminum camera tube (black painted, 20 mm i.d., length adjustable from 190 to 210 mm) was used. At the fall tube end, an achromatic lens (Oriel, model 42525, focal length 60 mm, 1 in. diameter) was mounted, and at the CCD end the camera tube was connected to the CCD with a bayonet mount.

The optical magnification of the lens/camera tube system was 3.1. The image distance $S2$ was the 200-mm camera tube length plus 35 mm (distance of the CCD imaging chip from the bayonet holder), and the object distance (lens to droplet) $S1$ was 75 mm; $S2/S1 = 3.1$. This was confirmed by imaging a grid of known spacing. The CCD chip had 384 × 576 pixels, each 23 × 23 μm. The image of a droplet on the CCD chip was 68–70 pixels (approximately 1600 μm) in diameter; this number of pixels is sufficient to resolve the temperature distribution within a droplet.

A biprism [fused silica, 50 mm diameter, 1.7-deg base angle (the angle between the flat side and either angled side), Atlantic Industrial Optics; antireflection coated, CVI Laser] in front of the CCD lens converted the droplet image into two images. The bandpass filters were immediately behind the biprism. The 1-in.-diam filter assembly consisted of two semicircular interference filters (CVI Laser): one centered at 450 nm (blue band) and the other centered at 550 nm (orange band), both with 70-nm FWHM bandpass. The biprism and the combined filter were mounted in a single holder that maintained their positions parallel to and coaxial with each other. Because the filters blocked both UV and red wavelengths, the background that resulted from the YAG and the heater incandescence was significantly reduced.

An electric shutter (Uniblitz, 100-2B, 1-in. aperture) was attached to the biprism–filter assembly, in front of the biprism. The shutter was opened and closed in 10 ms, which was $\frac{1}{10}$th of the 100-ms minimum exposure time of the CCD, and thus the shutter reduced the heater incandescence that was detected by the CCD by approximately a factor of 10. The shutter also isolated the prism and filter from the heat of the hot fall tube, a necessity because the bandpass of the interference filters is sensitive to temperature. Even so, to protect the prism and filter from heat, a small fan always circulated air between the shutter and fall tube and kept the temperature behind the shutter below 32°C.

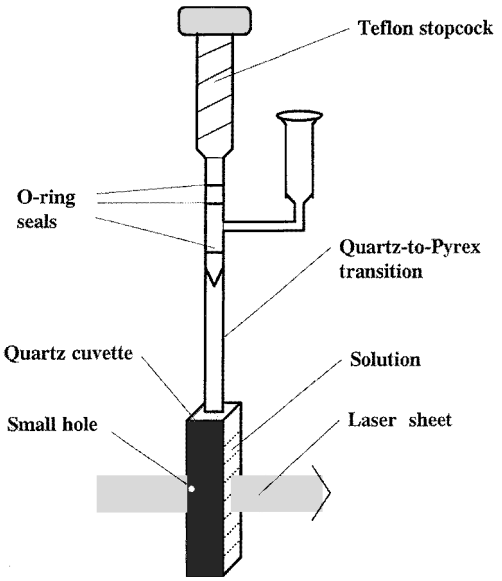

Fig. 5 Sealed cuvet used for temperature calibration.

6. Cuvet for Temperature Calibration

The apparatus is shown in Fig. 5. One side of the sealable quartz cuvet was painted black except for one small hole (about 0.5 mm diameter). Because the 1×10^{-4} M PYPYP/decane solution was optically thick for distances greater than 1 mm, most of the fluorescence originated near the front face of the cuvet, so that the small hole was set close to the side into which the laser sheet entered.

D. Droplet Solution and Choice of FST System

1. Choice of Concentration

Winter and Melton[18] showed that for reasonably uniform illumination of the equatorial section of a droplet, the DOD (equal to molar absorptivity × concentration × diameter) of the droplet should be approximately unity. The molar extinction absorptivity of PYPYP in decane at 266 nm, as measured on a UV/Vis spectrometer (Hitachi U-2000), was about 8×10^4 l/mol·cm. Thus, with a 500-μm-diam droplet, DOD = 1 required that the PYPYP concentration should be 2.5×10^{-4} M, which was close to the saturation limit of PYPYP in decane (about 2.7×10^{-4} M). In addition, at concentrations close to 5×10^{-4} M, exciplex formation may occur between pyrene moieties on different PYPYP molecules.[21] Therefore, a concentration of 1×10^{-4} M (DOD = 0.4) was used.

2. Oxygen Quenching of Fluorescence

In principle, FST systems other than PYPYP could have been used, and several FST systems that are insensitive to oxygen quenching (a problem with PYPYP[14]) have been studied. However, all of the FST systems that are insensitive to oxygen are also much less soluble in decane, and their use would have resulted in DOD values that were unacceptably small.[20] If oxygen was present within

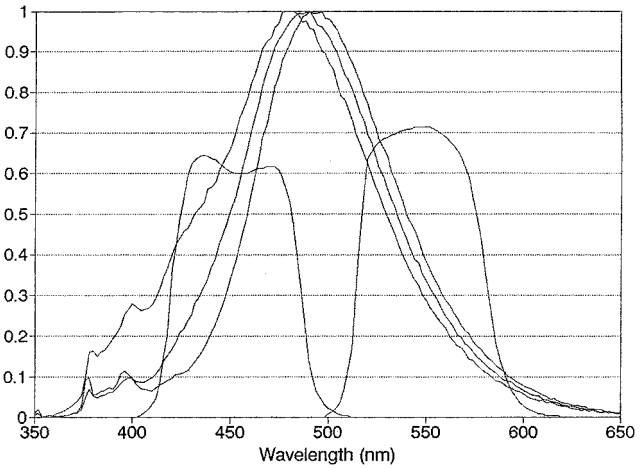

Fig. 6 Selected spectra of PYPYP as a function of temperature and transmission curves of interference filters.

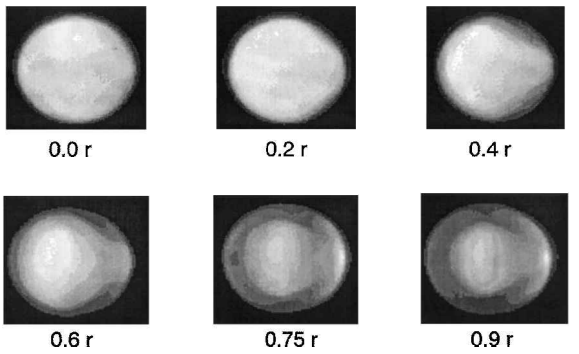

Fig. 7 Images as a function of distance of laser sheet from equatorial plane of droplet; lighter-gray-scale areas are higher fluorescence intensity.

or around the PYPYP/decane droplet, darker zones could be seen on the image, similar to those described by Winter and Melton.[18] Typically, when the nitrogen flow through the fall tube was started, the droplet image intensity was low, and as the oxygen was purged out of the fall tube, the intensity increased to a steady-state value.

3. FST Spectra and Band Ratios

The PYPYP excimer emission spectrum is in the wavelength range 360–650 nm, with the maximum intensity at about 480–500 nm. The excimer band shifts to shorter wavelength (blue shift) as the temperature increases, the basis for FST. Temperature-dependent fluorescence spectra of PYPYP and the approximate transmission curves for the two interference filters are shown in Fig. 6. Spectra are at 26, 90, and 170°C (from the right) and are normalized so that the maximum value is 1. Transmission curves are not normalized; the ordinate shows the fractional transmission of the filters.

The blue band and orange band filter bands, centered at 450 nm and 550 nm, respectively, were chosen to maximize the temperature-induced change in the relative ratio (RR) (see Sec. II.F.) while maintaining comparable, that is, within a factor of 2–3, intensity levels in both bands. A narrower bandpass for the filters would yield a steeper slope of RR vs T, that is, a more sensitive FST, but the decreased intensity would have made the experiment infeasible.

E. Basic Operation Procedures

1. Purging with Nitrogen

To eliminate (potentially irreproducible) fluorescence quenching effects associated with unknown concentrations of oxygen, nitrogen flows were used to purge oxygen from the system. The PYPYP solution was purged by bubbling nitrogen through the solution, and a small purging flow was maintained during a set of experimental runs. The empty droplet generator was purged with nitrogen, filled with purged solution, and inserted into the cold stage. A nitrogen flow was used to purge oxygen from the fall tube and was maintained for the duration of the experiment.

2. Alignment

Alignment of the laser sheet to illuminate the equatorial plane of the droplet is crucial. The initial alignment was carried out with the heaters off and the biprism/filter assembly removed. The droplet generator was aligned so that the droplets fall through the cold stage and fall tube with the minimum lateral movement. The laser time delay, laser sheet position, and camera tube optics were then set so that the falling droplet was illuminated, and the droplet was imaged on the CCD with the (single) droplet image on the midportion of CCD. With good alignment, the lateral deviation of droplet images as a function of fall distance was less than two droplet diameters over a fall distance of 7 cm.

The laser sheet was then aligned so that it illuminated the equatorial plane of the droplet. This was carried out by adjusting the laser sheet position relative to the droplet, taking CCD images, and comparing those images with ideally centered images, a technique first described by Winter.[22] The droplet surface acts like a lens, and it bends the incident rays. If the laser sheet slices exactly through the equatorial plane of the droplet, the droplet fluorescence makes it appear that the droplet is illuminated nearly homogeneously. When the incident laser sheet is offcenter, increasing deviations appear. Figure 7 shows a series of such images, which were captured under conditions in which internal circulation was negligible.

Once the laser sheet was aligned with respect to the droplet, the biprism/filter assembly was replaced, and the biprism/filter assembly prism was rotated so that the dual images appear at the same horizontal positions on the CCD monitor. It was difficult to replace the assembly exactly, and invariably the images fell on slightly differing sets of pixels each time the assembly was adjusted. For this reason, the RR (see Sec. II.F.) was adopted for analysis of the images.

3. Droplet Images Required

To provide appropriate images for the ratios required (see Sec. II.F) both room temperature and elevated temperature (of the gas) images must be recorded. Room temperature images were recorded at $z = 15$ mm. After the room temperature images were recorded, the heaters were turned on, and the laboratory jack was adjusted to move the fall tube apparatus in approximately 5-mm increments from $z = 5$ to 70 mm and, thus, obtain images at a sequence of fall times.

F. Image Processing

For image processing, the orange and blue CCD images were saved separately as 100×100 pixel arrays. The average background was subtracted, and the binary format images were converted to American Standard Code for Information Interchange (ASCII) format. Typical signals were 200–500 counts per pixel in the droplet image, with background levels of approximately 50 counts per pixel.

A determination of the pixel that defines the edge of each droplet image was necessary to prepare the images for pixel-by-pixel ratioing, and this determination introduced some arbitrariness into the procedure. Uncertainties of 1 pixel were routine; uncertainties of 2 pixels were much less common.

Four files were processed to yield one temperature field image for a droplet. At ambient temperature T, the integrated intensity of the orange band (515–585 nm) at pixel (i, j), $E1(T, i, j)$, was divided by the integrated intensity of the blue band (415–485 nm), $E2(T, i, j)$, to form the ratio $R(T, i, j) = E1(T, i, j)/E2(T, i, j)$. The $\mathrm{RR}(T, i, j)$ is

$$\mathrm{RR}(T, i, j) = R(T, i, j)/R(\mathrm{RT}, i, j) \tag{1a}$$

$$\mathrm{RR}(T, i, j) = [E1(T, i, j)/E2(T, i, j)]/[E1(\mathrm{RT}, i, j)/E2(\mathrm{RT}, i, j)] \tag{1b}$$

$$\mathrm{RR}(T, i, j) = [E1(T, i, j)/E1(\mathrm{RT}, i, j)]/[E2(T, i, j)/E2(\mathrm{RT}, i, j)] \tag{1c}$$

where RT is room temperature. As shown in Eq. (1c), for images processed in this manner, the pixel-to-pixel variations in sensitivity were ratioed out.

The spherical surface of a droplet refracted the outgoing fluorescence and distorted the image recorded by the CCD camera. Zhang and Melton[16] analyzed the optics of a droplet and the formation of laser droplet-slicing image; they provided a package of programs to partially restore the image. The best procedure for processing the images was to restore each image using the Zhang and Melton programs and then calculate RR(T, i, j) using the restored images. The use of restored images made it clear that, because of the lensing effects of the droplet (center portion the image was expanded, outer portion was compressed), only the inner 60% of the droplet image yielded interpretable temperature measurements.

Once the image of RR(i, j) had been calculated, it was converted to a temperature image $T(i, j)$ by use of a lookup table derived from the temperature calibration curve (Fig. 8).

G. Temperature Calibration

The temperature calibration was carried out with exactly the same optics and data processing that was used for the actual droplet imaging. The inner fall tube, cold stage, and top ceramic cover were removed, and the cuvet assembly was inserted vertically into the fall tube, its black side toward the CCD camera. The top of the fall tube was covered with two pieces of half-square ceramic plates. With the same light source and optics (lens, biprism, and filters) as used for droplet imaging, dual images of the small hole were obtained from RT to the maximum droplet temperature expected (normal boiling point for decane = 174°C) with 40 min allowed for equilibration at each temperature. The intensity was calculated as the average (background subtracted) intensity for a 10 × 10 square of pixels from the central portion of each image.

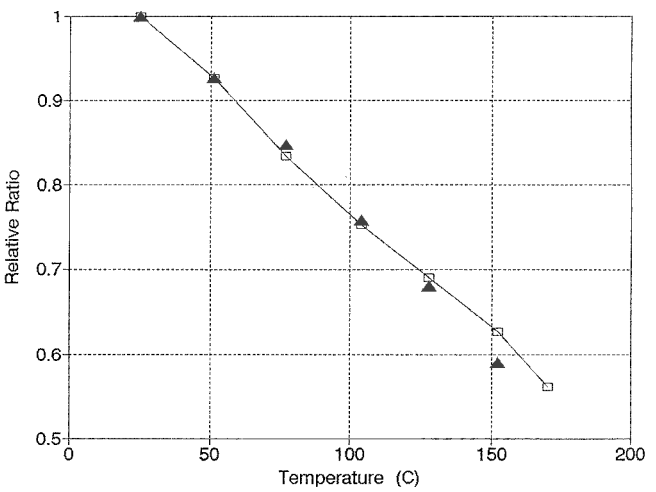

Fig. 8 Temperature calibration: RR vs T.

III. Results and Discussion

A. Temperature Calibration

The calibration curve, RR(T) vs T, is shown in Fig. 8. The two sets of data points show results obtained with independent runs on successive days. The graph shows modest curvature, and, indeed, there is no theoretical reason to expect that it should be linear. Fluorescence shift thermometers, which are highly robust (insensitive to perturbations in the environment, excitation and collection optics, etc.) have limited sensitivity and dynamic range. The average slope for Fig. 8 is 3.1×10^{-3}/°C. The uncertainty in the individual points ($2s$, 90% confidence level) is approximately ±0.02. Thus, the minimum resolvable temperature difference is approximately 6°C (slope/$2s$).

B. Images of Droplets

Figure 9 shows the temperature field as a function of fall distance within the heated fall tube. The droplet velocity is approximately 1.8 m/s (=1.8 mm/ms). The temperature in the fall tube was not homogeneous, and the temperature indicated on each image is the measured gas temperature at that point in the fall tube. The intensity images were restored by the procedures given by Zhang and Melton,[16] and RR (i, j) was calculated from the restored images.

As already stated, fluorescence from an equatorial plane of the droplet is excited by the laser sheet, and the fluorescence image that actually reaches the CCD camera plane is significantly distorted by refraction. The central portion expands almost linearly, and the fluorescence originating in the outer 40% of the droplet radius is compressed into a narrow shell at the edge of the DSI image. Accurate restoration of the inner 60% of the original fluorescence pattern is straightforward; restoration of the outer 40% is difficult at best, and with less than excellent signal to noise, as was the case in this work, it is impossible.

The diameter of the raw images remains constant, within a resolution of 1–2 pixels, as a function of fall distance in the heated zone. However, Wells and Melton[13] argued that thermal expansion must be taken into account when using the diameter of a heating droplet to assess the amount of evaporation. If the droplets that have fallen 70 mm are assumed to have an average temperature of 150°C, then the liquid phase density will have dropped by about 15% from the RT liquid density,[23] and thus a constant diameter implies a 15% reduction in the droplet mass, that is, 15% evaporation.

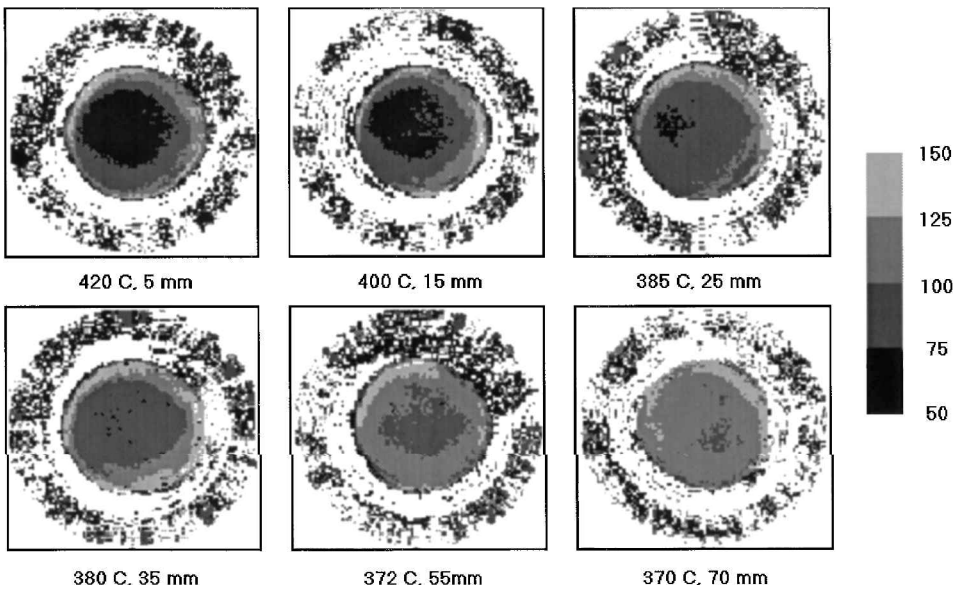

Fig. 9 Restored images of temperature field within 0.5-mm-diam droplet as a function of fall distance in 400°C nitrogen.

The temperature field images in Fig. 9 show no evidence of internal circulation.[18] Rather, they show a generally homogenous core, which rises in temperature as the droplet falls through increasing distance, that is, increasing time, in the heated nitrogen. At $z = 5$ mm the core temperature is already in the 50–75°C range; at $z = 35$ mm, it is 75–100°C; and at $z = 70$ mm, it is 100–125°C. The surface temperature, which could not be imaged, is, of course, higher.

Zhang and Melton argued that, if the CCD camera were placed at an angle other than 90 deg to the plane of the laser sheet, then the near side of the image could be accurately restored at the cost of less information about the far side of the droplet.[16] After the images shown in Fig. 9 were obtained, such imaging experiments were attempted. The CCD camera was placed on a tiltable platform, and the axis of the camera tube was elevated 30 deg, as recommended by Zhang and Melton.[16] Initial images were obtained as a function of fall distance in the heated tube, but substantial imaging problems (primarily associated with the proper focusing of the vertical image plane in the droplet) were never resolved.

The RT droplets have fallen approximately 20 mm through the cooling stage when they reach the heated zone, and the Winter and Melton[18] results would suggest that they already have a well-established internal flowfield at the time that they enter the high temperature zone. Thus, the likely existence of a prior internal flowfield coupled with the inability to capture the temperature field near the surface make these images problematic for spray modeling purposes. It may be necessary to adapt techniques that probe the surface region specifically.[24] It is hoped that others interested in the droplet and spray area will be able to use the apparatus, techniques, and results from this work to better resolve the issues surrounding the rapid heating of droplets generated in a fuel spray.

IV. Conclusions

The experiments described in this paper ended prematurely, and consequently a full range of investigations of the transient heating behavior of falling droplets was not conducted. The sequences of droplet images that were analyzed indicate that heat transfer into the center of the droplets is sufficiently rapid that careful calculation of internal circulation effects is not necessary; this conclusion should be investigated under a wider range of initial conditions. The experimental section describes the constraints and adaptations that led, ultimately, to a working apparatus, and it is hoped that others will find that this work makes similar measurements easier to carry out.

Acknowledgments

The support of the U.S. Army Research Office through Grant DAAH04-94-G-0020 is gratefully acknowledged.

References

[1]Elperin, T., and Krasovitov, B., "Analysis of Evaporation and Combustion of Random Clusters of Droplets by a Modified Method of Expansion into Irreducible Multipoles," *Atomization and Sprays*, Vol. 4, No. 1, 1994, pp. 79–97.

[2]Sirignano, W. A., and Bhatia, R., "Metal Slurry Droplet and Spray Combustion," *Advances in Combustion Science: In Honor of Ya. B. Zel'dovich*, edited by W. A. Sirignano, A. G. Merzhanov and L. De Luca, Vol. 173, Progress in Astronautics and Aeronautics, AIAA, Reston VA, 1997, pp. 117–130.

[3]Wong, S.-C., Liao, X.-X., and Yang, J.-R., "A Simplified Theory of the Ignition of Single Droplets Under Forced Convection," *Combustion and Flame*, Vol. 110, No. 3 , 1997, pp. 319–334.

[4]Bhattacharya, P., Ghosal, S., and Som, S. K., "Evaporation of Multicomponent Liquid Fuel Droplets," *International Journal of Energy Research*, Vol. 20, No. 5, 1996, pp. 385–398.

[5]Bellan, J., and Harstad, K., "Ignition of a Binary Fuel (Solvent-Solute) Cluster of Drops," *Combustion Science and Technology*, Vol. 110/111, 1995, pp. 531–548.

[6]Zhang, J.-J., Yukao, C.-Y., Ho, J.-T., and Wong, S.-C., "Experimental Study of the Ignition of Single Droplets Under Forced Convection," *Combustion and Flame*, Vol. 110, No. 3, 1997, pp. 366–376.

[7]Ondas, M. S., and Santavicca, D. A., "A Study of Droplet Vaporization in a Longitudinal Acoustical Field Using Exciplex Vapor/Liquid Visualization," *Proceedings of the ASME Fluids Engineering Division*, ASME FED-Vol. 244, American Society of Mechanical Engineers, Fairfield, NJ, 1997, pp. 159–166.

[8]Tsue, M., Kadota, T., Segawa, D., and Yamasaki, H., "Statistical Analysis on Onset of Microexplosion for an Emulsion Droplet," *Symposium (International) on Combustion*, Vol. 26, Combustion Inst., Pittsburgh, PA, 1996, pp. 1629–1635.

[9]Luczak, A., Eisenberg, S., Schluter, H., Beushausen, V., and Andresen, P., "3-D Density and Temperature Measurements in an Oil Spray Flame Using Ultraviolet Raman Scattering," *Air Pollution and Visibility Measurements*, Proceedings, Vol. 2506, Society for Photo-Optical Instrumentation and Engineering, Bellingham, WA, 1995, pp. 121–131.

[10]Melton, L. A., "Use of Fluorescence Methods for Measurement of Droplet and Vapor Temperatures," *Recent Advances in Spray Combustion: Spray Combustion Measurements and Model Simulation. Volume II*, edited by K. K. Kuo, Vol. 171, Progress in Astronautics and Aeronautics, AIAA, Reston, VA, 1996, pp. 143–158.

[11]Sankar, S. V., Buermann, D. H., and Bachalo, W. D., "Application of Rainbow Thermometry to the Study of Fuel Droplet Heat-Up and Evaporation Characteristics," *Journal of Engines, Gas Turbines, and Power*, Vol. 119, No. 3, 1997, pp. 573–584; also American Society of Mechanical Engineers, Paper 96-GT-21, June 1996.

[12]Schaller, J. K., Wassenberg, S., and Stojanoff, C. G., "A New Method for Temperature Measurements of Droplets," *Laser Applications in Combustion and Combustion Diagnostics II*, Proceedings, Vol. 2122, Society for Photo-Optical Instrumentation and Engineering, Bellingham, WA, 1994, pp. 186–194.

[13]Wells, M. R., and Melton, L. A., "Temperature Measurements of Falling Droplets," *Journal of Heat Transfer*, Vol. 112, No. 4, 1990, pp. 1008–1013.

[14]Hanlon, T. R., and Melton, L. A., "Exciplex Fluorescence Thermometry of Falling Hexadecane Droplets," *Journal of Heat Transfer*, Vol. 114, No. 2, 1992, pp. 450–457.

[15]Zhang, J., and Melton, L. A., "Potential Systematic Errors in Droplet Temperatures Obtained by Fluorescence Methods," *Journal of Heat Transfer*, Vol. 115, No. 2, 1993, pp. 325–331.

[16]Zhang, J., and Melton, L. A., "Numerical Simulations and Restorations of Laser Droplet-Slicing Images," *Applied Optics*, Vol. 33, No. 2, 1994, pp. 192–200.

[17]Winter, M., "Measurement of the Temperature Field Inside a Falling Droplet," *Extended Abstracts*, 4th Annual Conf., Inst. for Liquid Atomization and Spray Studies, UCI Combustion Lab., Univ. of California, Irvine, CA, 1990.

[18]Winter, M., and Melton, L. A., "Measurement of Internal Circulation in Droplet Using Laser-Induced Fluorescence," *Applied Optics*, Vol. 29, No. 31, 1990, pp. 4574–4577.

[19]Harris, S. R., Lempert, W. R., Hersh, L., Burcham, C. L., Saville, D. A., Miles, R. B., Gee, K., and Haughland, R. P., "Quantitative Measurements of Internal Circulation in Droplets Using Flow Tagging Velocimetry," *AIAA Journal*, Vol. 34, No. 3, 1996, pp. 449–454; also AIAA Paper 95-0168, Jan. 1995.

[20]Bai, F., and Melton, L. A., "High-Temperature, Oxygen-Resistant Molecular Fluorescence Thermometers," *Applied Spectroscopy*, Vol. 51, No. 9, 1997, pp. 1276–1280.

[21]Gossage, H. E., and Melton, L. A., "Fluorescence Thermometers Using Intramolecular Exciplexes," *Applied Optics*, Vol. 26, No. 11, 1987, pp. 2256–2259.

[22]Winter, M., "Droplet Slicing Measurements of Internal Circulation," AIAA Paper 93-0900, Jan. 1993.

[23]Gallant, R. W., and Railey, J. M., *Physical Properties of Hydrocarbons*, Vol. 3, Gulf, Houston, TX, 1984, p. 124.

[24]Chen, G., Mazumder, M. M., Chang, R. K., Swindal, J. C., and Acker, W. P., "Laser Diagnostics for Droplet Characterization: Application of Morphology Dependent Resonances," *Progress in Energy and Combustion Science*, Vol. 22, No. 2, 1996, pp. 163–188.

R. P. Lucht
Associate Editor